Measurement of Lagrangian Acceleration Using the Laser Doppler Technique

Matthias Kinzel[1,2], Holger Nobach[1,3], Cameron Tropea[2], Eberhard Bodenschatz[3]

[1]Laboratory of Atomic and Solid State Physics (LASSP), Cornell University, Ithaca NY, USA;
[2]Chair of Fluid Mechanics and Aerodynamics (SLA), Technische Universitaet Darmstadt, Germany;
[3]Max Planck Institute for Dynamics and Self-Organization, Göttingen, Germany

ABSTRACT

This paper deals with an extension of the laser Doppler technique for measuring Lagrangian acceleration. First the optical design and the accurancy requirements for its alignment are introduced. Next the data post processing that extracts the velocity and acceleration information from the measurement data is explained. Then a method to validate the alignment of the optical components is presented. Finally, two experiments that were done to validate the acceleration measurements with the LDA method are presented and their results are discussed.

1 INTRODUCTION

Knowledge of the Lagrangian or material acceleration is very valuable in fluid mechanics as the fundamental conservation equations are cast in terms of this acceleration, in particular the Navier-Stokes equations. This is especially true for turbulent flows where physical effects must often be modelled for simulation or predictive purposes. Little experimental data exists on the material acceleration in turbulent flows, primarily due to the difficulty of measurement. The methods used to date were particle tracking with high-speed cameras (N. T. Ouellette et al. 2005) or silicon strip detectors (G. A. Voth et al., 2001; A. La Porta et al., 2001; G.A. Voth et al., 2002). However, the laser Doppler technique offers also an alternative method, as demonstrated by Lehmann et al. (1990); Lehmann and Helbig (2000) and Lehmann et al. (2002). A comparison between techniques is important to evaluate the accuracy of the data obtained from both techniques.
Due to the properties of the laser Doppler system there are some differences compared to the high-speed particle tracking. The size of the measurement volume of the laser Doppler system is only of the order of 100µm and the time a particle typically resides in the measurement volume is about 1µs. Thus the measurement must be considered as a point measurement. The consequence is that the measured quantities are Lagrangian but the statistics gained from this data are Eulerian. In the particle tracking systems the measurement volume is relatively large allowing the path of a particle to be tracked over a certain time. Because of this the statistics of the Lagrangian acceleration measured with the particle tracking techniques are also Lagrangian. As one statistic is Eulerian and one is Lagrangian they can not be directly compared, but the probability density functions of the Lagrangian acceleration measured with the two different techniques can be.

This manuscript describes in the following section the optical system used to perform the laser Doppler acceleration measurements, followed by a section detailing the signal processing required to estimate the acceleration from the received Doppler signal. In section 4 reference measurements using a moving wire in the measurement volume are presented and used for validation of the technique, followed by measurements from a particular flow in which also high-speed strip detectors were used. The manuscript concludes with several overall statements regarding the feasibility of this technique for examining turbulent flows.

2 OPTICAL DESIGN

2.1 Optical Components

One aim of this project was to achieve acceleration measurements with a commercial laser Doppler system. By using a commercial system this demonstrates immediately the potential for upgrading existing laser Doppler systems for such measurements.
The optical setup used is a standard three-velocity component laser Doppler system from TSI as shown in Figure (1), although only one component was actively used. For this component the 514.5 wavelength band of a 5W

Argon-Ion laser was used. The transmitting lens has a focal length of 363mm and the receiving lens of 20mm. In this setup the signal processor is not used except to provide the frequency shift signal f_{sh} for the Bragg cell.

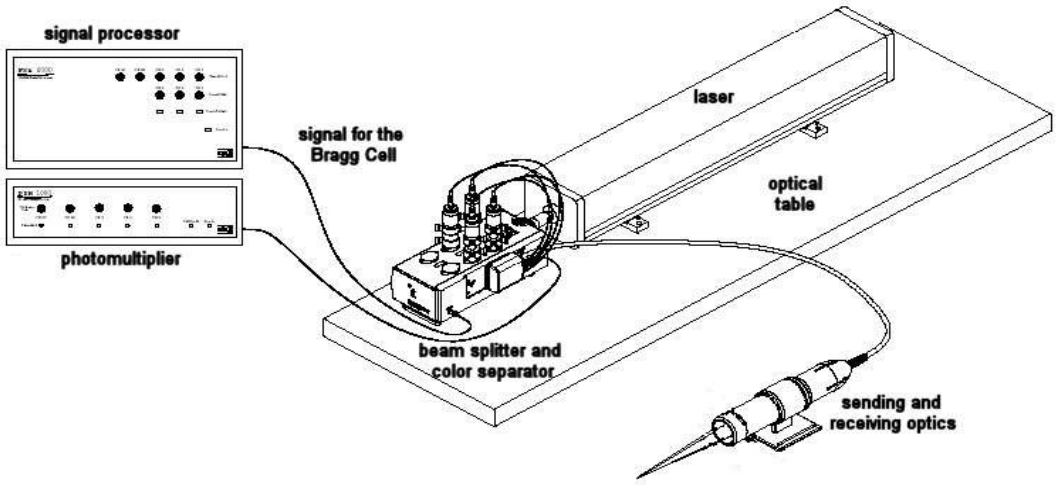

Figure 1: Optical components of the laser Doppler system

2.2 Accuracy of the optical alignment

Due to the small size of the measurement volume the expected changes of velocity within the measurement volume is small. With a typical measurement volume diameter of 100µm and a typical particle mean velocity and acceleration in a turbulent flow of 10m/s and 1000m/s² respectively, the expected change in velocity is only 0.1%. Therefore the optical alignment must be very accurate to be able to measure this small change. To achieve this, the fringe divergence in the measurement volume must be made as small as possible. The fringe divergence is caused by the fact that the planes of constant phase in the Gaussian laser beams are curved as shown in Figure (2).

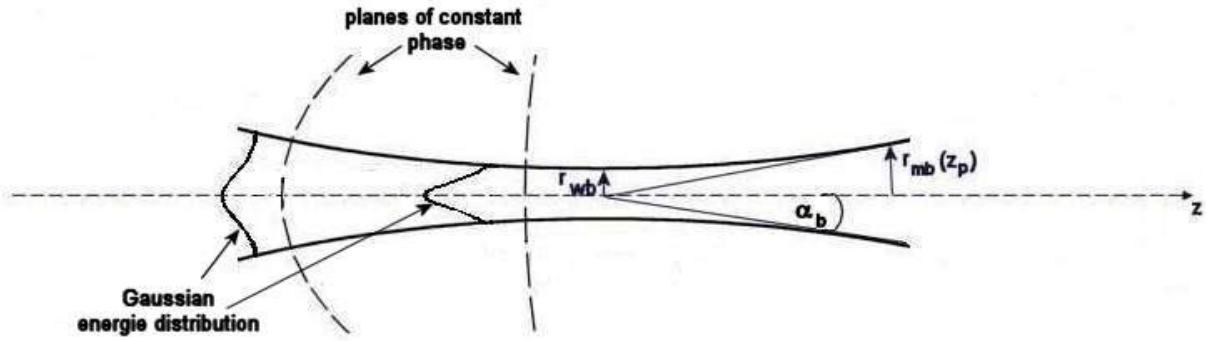

Figure 2: Gaussian laser beam

In this graphic $r_{mb}(z)$ is the laser beam radius as a function of the z-position, r_{wb} is the beam waist radius and α_b is the divergence angle of the beam. The planes of constant phase are plotted as dashed lines and the Gaussian energy distribution in x-direction is shown as solid curves.
As the planes of constant phase are curved, there is always some fringe divergence even in a perfectly aligned system. Figure (3a) displays this divergence.

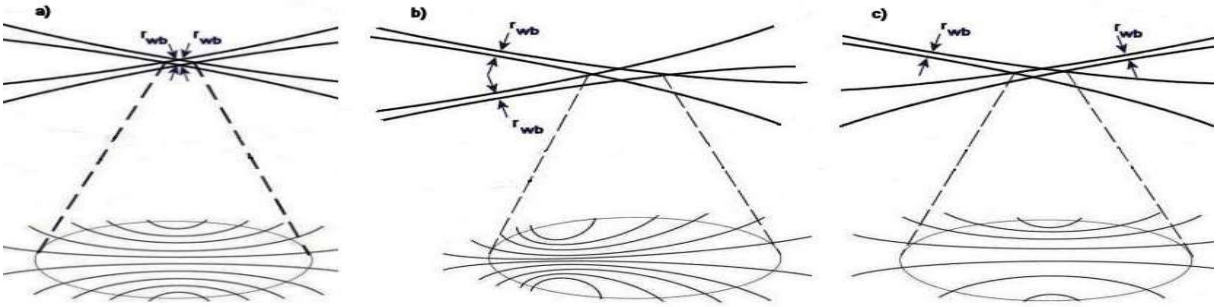

Figure 3: Fringe divergence in the measurement volume

The position of each beam waist cannot be adjusted with an accuracy better than about +/- 150µm using a pinhole and a powermeter. Hence there are two more kinds of fringe divergence that may occur in the measurement volume. The first results if both beam waists are misaligned in the same z-direction, and the second if the two beam waists are misaligned in opposite z-directions. The fringe divergence caused by these misalignments is shown in the figures (3b) and (3c). As the radius of the planes with constant phase becomes smaller with distance to the beam waist, the maximum fringe divergence occurs at the boundaries of the measurement volume.
Albrecht et al. give equation (1) for the fringe divergence in the measurement volume as a function of the beam waist positions of the two laser beams that create the fringe system.

$$\Delta x = \frac{\lambda_b}{2\sin\left(\frac{\Theta}{2}\right)}\left(1-\frac{\frac{x_1 z_1}{{z_1}^2+{l_{R1}}^2}-\frac{x_2 z_2}{{z_2}^2+{l_{R2}}^2}}{2\tan\left(\frac{\Theta}{2}\right)+\left(\frac{x_1 z_1}{{z_1}^2+{l_{R1}}^2}-\frac{x_2 z_2}{{z_2}^2+{l_{R2}}^2}\right)}\right) \qquad (1)$$

Figure (4) displays a schematic picture of the measurement volume and in table (1) its dimensions are given.

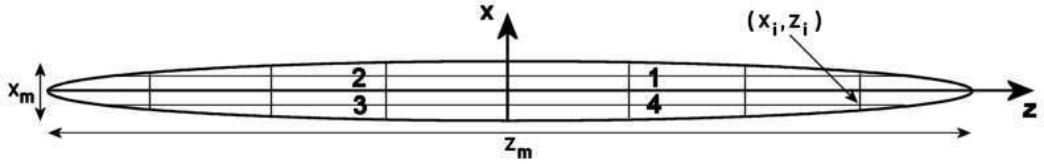

Figure 4: Grid for divergence calculation

The grid in Figure (4) marks the points where the fringe divergence was calculated.

x_m [µm]	68,1
y_m [µm]	68
z_m [µm]	988,8
Δx [µm]	3,7441
N_{fr}	18

Table 1: Dimensions of the measurement volume

x_m, y_m and z_m are the maximum diameters of the measurement volume in these directions. Δx is the fringe spacing and N_{fr} is the number of fringes in the measurement volume. With these dimensions and the beam waist misalignment of 150µm a maximum fringe spacing of 3.7608µm is obtained from equation (1). This corresponds to a change in the divergence of 0.05% compared to the value given in table (1). Hence the equations (2) and (3) that are used to calculate the velocity and the acceleration are linearly dependent on the fringe spacing. In these equations γ is the parameter of the model signal for the acceleration, f_d is the Doppler frequency and f_s is the shift frequency. The error that is caused by the fringe divergence is equal to or less than 0.05%.

$$a = \gamma \Delta x \qquad (2)$$

$$v = (f_d - f_{sh})\Delta x \qquad (3)$$

3 SIGNAL PROCESSING

3.1 Signal Generation

The TSI photomultiplier unit has 20MHz high-pass filters that filter the electrical signal from the photomultipliers. Thus the DC component of the burst signal is removed, making the signal symmetric about zero, as shown in Figure (5b). The frequency of the signal, the so called Doppler frequency f_d, is of the order of the Bragg cell frequency f_s, which is 40MHz. To be able to see the characteristics of a Burst signal a simulated burst signal with a frequency of only 500kHz is displayed in Figure (5a).

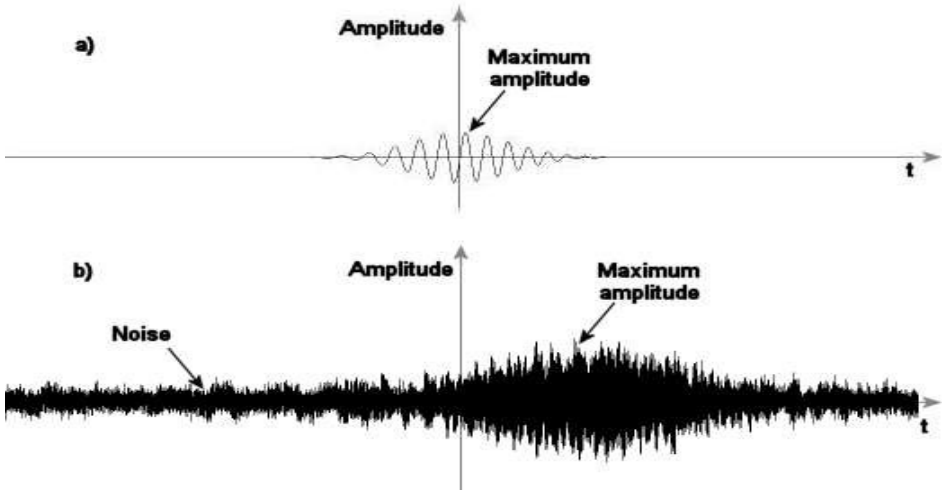

Figure 5: Simulated and measured burst signals

Because of the lower frequency, the oscillations that are caused by the tracer particles crossing the fringe system and the increase of the frequency within the signal are visible. The Doppler frequency of the signals is directly dependent on the particle velocity as shown in equation (3). Hence the change in the frequency is due to the acceleration of the tracer particles. Equation (2) describes the relation between the acceleration and the frequency change. The Gaussian shape of the amplitudes envelope is caused by the Gaussian energy distribution in the x-direction of the laser beams (Figure (2)). Because of the noise, there is more than just the frequency f_d in the measured signal, causing the irregular look.

3.2 Signal Processing

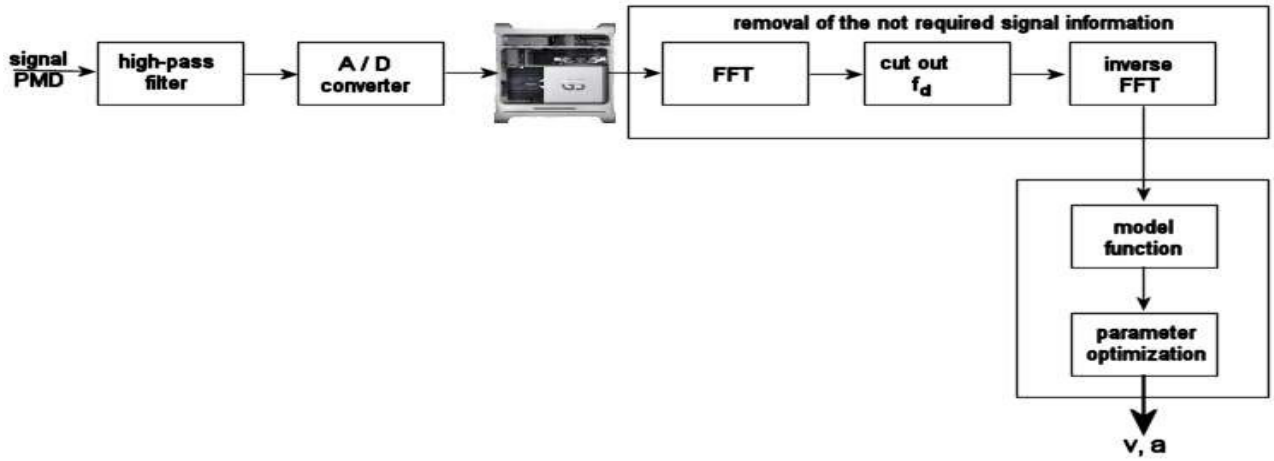

Figure 6: Flowchart of the signal processing

In Figure (6) the flowchart of the signal processing is presented. After the high-pass filter, the signal is digitized and stored. The sampling frequency of the data acquisition cards is 100MHz to make sure that aliasing effects do not occur. Due to the high data rates, the cards are equipped with 32MB on-board memory that allows 2000 burst signals to be recorded without interruption. The resolution of the cards is 14 bit and the input voltage range is 0 to 5V, adjustable in steps of 1 volt. Furthermore the burst arrival time is recorded.

The post-processing can be divided into two parts. In the first part the information required to estimate the velocity and the acceleration are extracted from the signal. Therefore, the burst signal $\hat{s}(t)$ is transformed into the amplitude spectrum using the fast Fourier transformation (FFT). The signal is then band-pass filtered in spectral domain before transforming back into time domain.
In the second stage of the processing the model signal given in equation (4) is fitted to the burst signal. This model function is bias free and consistent, almost achieving the Cramer-Rao lower bound.

$$s(t) = \cos\left(\pi\gamma(t_i - t_0)^2 + 2\pi t_i f_d\right) + i\sin\left(\pi\gamma(t_i - t_0)^2 + 2\pi t_i f_d\right) \quad (4)$$

As shown in equations (2) and (3), the Doppler frequency f_d and the parameter for the acceleration γ are to be estimated from the burst signal. The second part of equation (4) is a complex extension of the model which allows the model signal to account for arbitrary signal phase. The information about the Gaussian shape of the burst amplitude and the degree of modulation that are obtained in the burst signal are not very reliable measures due to noise and are therefore not taken into account.
The correlation between the model signal and the measured burst signal reaches its optimum when the product of both signals reaches its maximum.

$$R = \left|\sum s_i \hat{s}_i\right| \overset{!}{=} \max \quad (5)$$

For R to reach its maximum the first derivative of R must be zero.

$$\frac{\partial R}{\partial f_d} = 0; \quad \frac{\partial R}{\partial \gamma} = 0 \quad (6)$$

To find the points where these second derivatives are zero, a two-dimensional Newton approximation is used. As start values for this optimisation f_d is approximated by the formula given in equation (7) and γ is set to zero, since its probability density function is symmetric about zero.

$$f_d \approx \frac{f_s}{N_{samples}}\left(n + \frac{\ln(y_{n-1}) - \ln(y_{n+1})}{2(\ln(y_{n-1}) + 2\ln(y_n) + \ln(y_{n+1}))}\right) \quad (7)$$

In equation (7) f_s is the sampling frequency, $N_{samples}$ is the number of samples in the measured burst and *n* is the position of the maximum frequency in the amplitude spectrum of the burst. Thus the first part of the right-hand side of this equation represents the frequency of the burst signal that was found in the FFT. The second part of the right-hand side is introduced to approximate the exact value of the Doppler frequency, since this value can be slightly higher or lower than the one found by the Fourier analysis. The variables y_{n-1}, y_n and y_{n+1} are the values of the function given in equation (8) at the points n_{-1}, n and n_{+1}.

$$g(f_s) = \ln\left(\left|FFT(\hat{s})\right|\right) \quad (8)$$

With these start parameters the stop criterion of the optimization of R is reached within three to four iteration steps.
Figure (7) shows a burst signal and the model signal that was fitted to it. The three enlarged cut-outs show the correlation between the frequencies of the measured and the model signal.

4 ACCELERATION MEASUREMENTS

To validate the measurement procedure and the data processing two different experiments were performed. The aim of these experiments was to compare the measured acceleration to data that was obtained by calculations or with different measurement techniques.

4.1 Validations of the Optical Setup

For the first experiment a setup was realized that allows a thin metal wire to be dropped through the measurement volume. As the wire is approximately in free fall its acceleration is close to the acceleration of gravity and its velocity can be calculated out of this acceleration and the height of fall. Furthermore, the z-position where the wire crosses the fringe system can be adjusted to measure the acceleration and the velocity at different locations within the measurement volume. The data that is obtained at the different measurement positions yields information about the fringe divergence in the measurement volume. In this manner the accuracy of the fringe system in the measurement volume and therefore of the optical alignment can be validated.

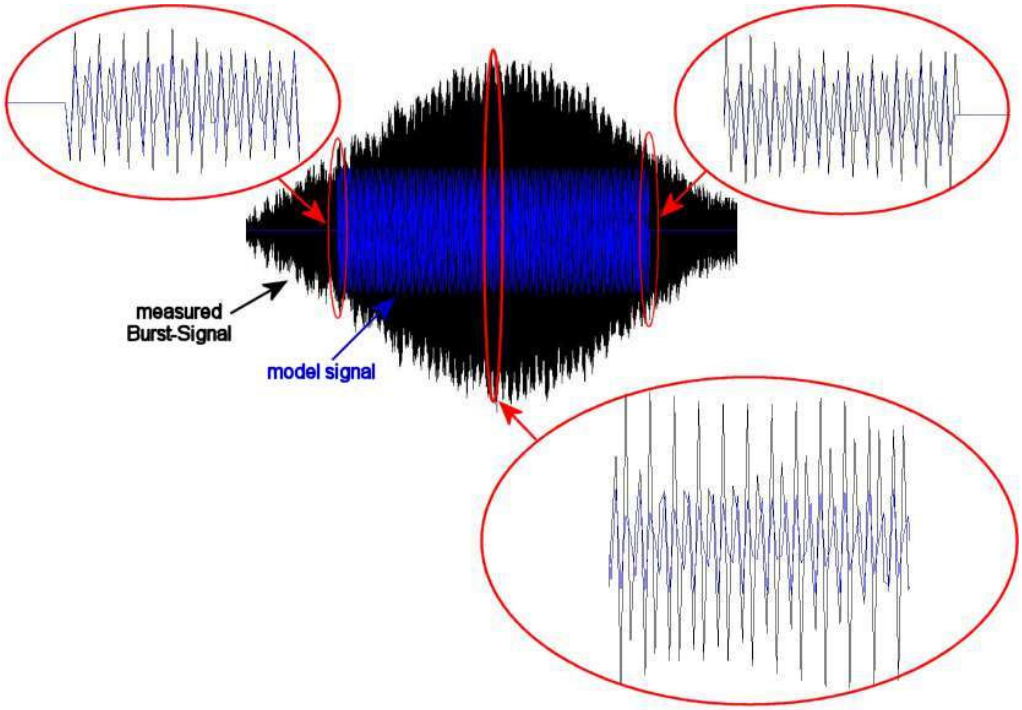

Figure 7: Comparison between the measured and the model signal

The experimental setup is shown in Figure (8). The wire is clamped between two screws that are mounted into the middle part of the construction. This middle bridge can slide up and down in the frame. At the top of the frame is a traversing system which allows exact positioning of the wire.

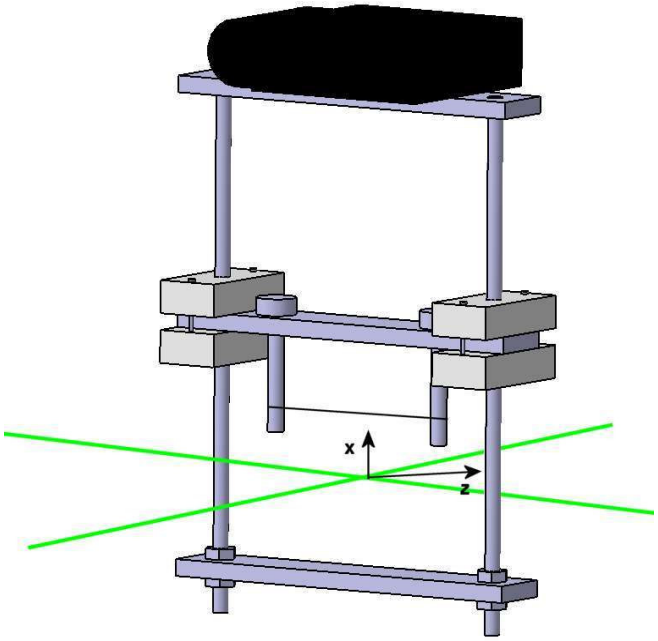

Figure 8: Setup of the falling wire experiment

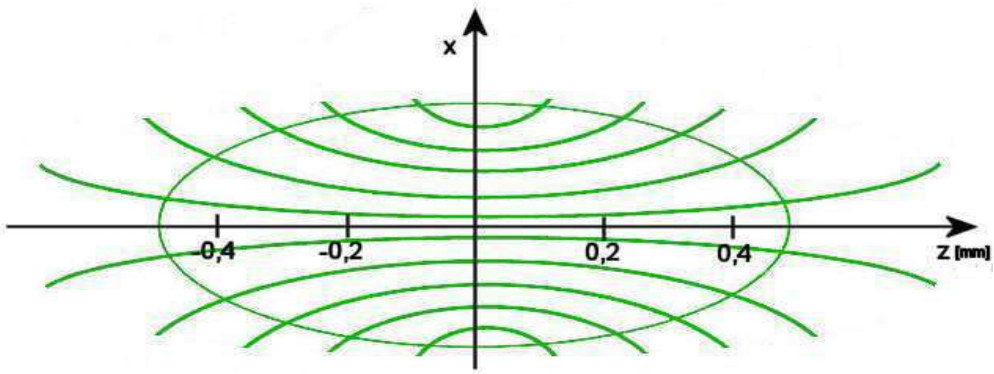

Figure 9: Measurement positions of the falling wire experiment

The five measurement positions are 200 µm apart from each other as shown schematically in Figure (9). At each position ten measurements have been analyzed. The falling height for this experiment was 55mm. The averaged velocities and accelerations from this experiment are plotted over the z-position in Figure (10).

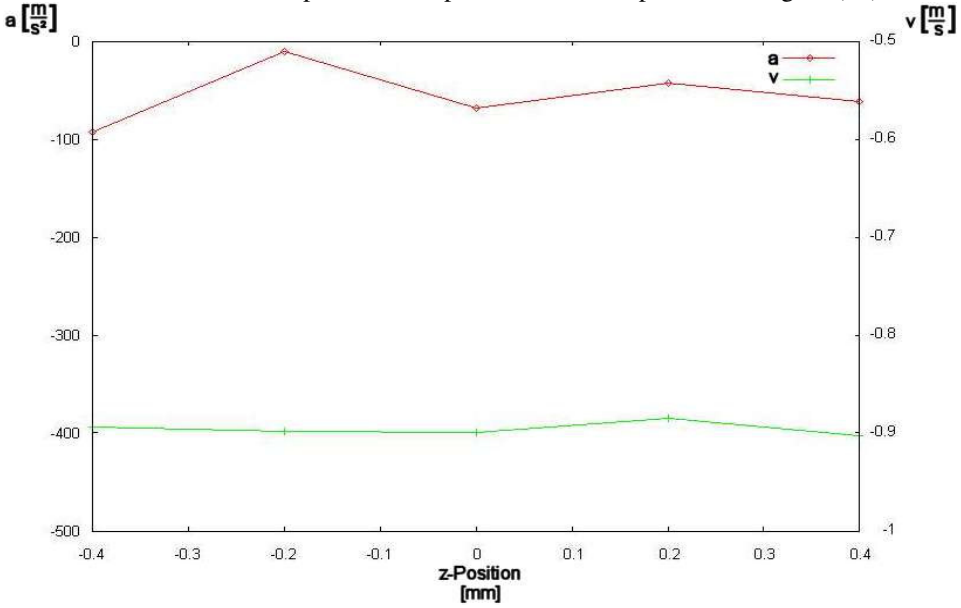

Figure 10: Results from the falling wire experiment

The left y-axis shows the acceleration values that belong to the curve with the diamond shaped dots and the right y-axis belongs to the velocity curve which is the one with the dashed marks. The wire velocity is very constant and though the acceleration curve looks a little uneven, there are no outliers observed. Therefore, this measurement validates the results from the calculation approach mentioned in section 2.2, namely that the fringe divergence can be neglected.
The Root Mean Square (RMS) value of the acceleration was found to be about 200m/s². This seems to be quite high, but considering the small change in the velocity within the measurement volume that must be estimated, this is a very low value. Moreover, the acceleration in turbulent flows can easily be of the order of 10^5 m/s² which makes a RMS value of about 200m/s² tolerable.

4.3 Lagrangian Acceleration Measurement

With the falling wire experiment the resolution of the acceleration measurement using the laser Doppler system has been determined. Next an experiment a turbulent a von Karman swirling water flow was investigated at a Taylor microscale Reynolds- number of approx. 500 to determine whether this resolution is sufficient to measure Lagrangian acceleration. Furthermore, a similar flow was independently measured using silicon strip detectors, allowing comparison to the laser Doppler measurements.

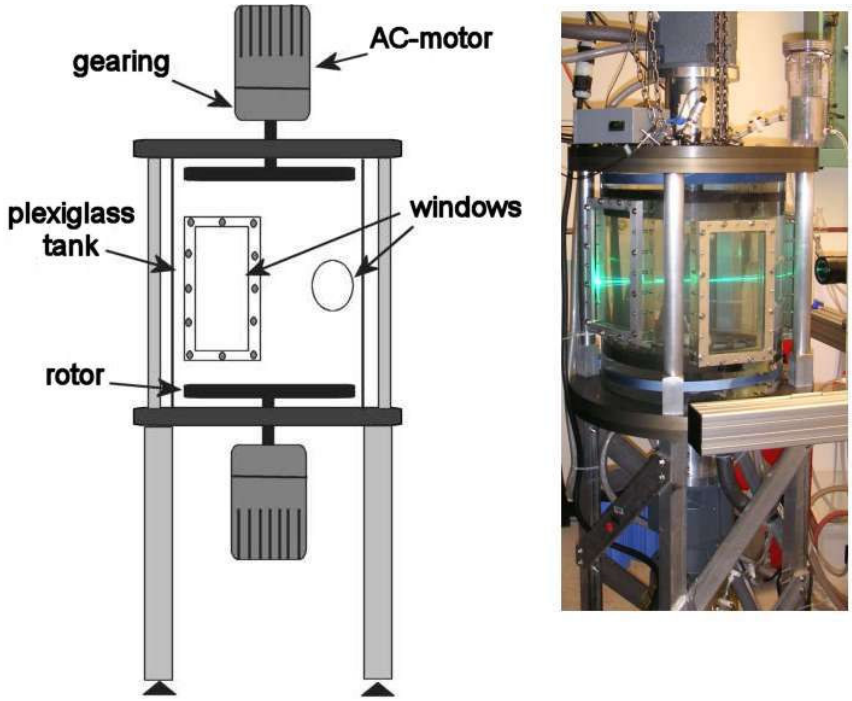

Figure 11: Turbulence generator (French washing machine)

In Figure (11) a schematic drawing and a photograph of the turbulence generator are shown. The turbulent flow is generated in a cylindrical tank made out of acrylic glass. The diameter of the tank is 437mm and its height is 605mm. In the walls of the tank there are five windows that allow optical access. The flow is created by one rotor that is located at the top and another rotor that is located at the bottom of the tank. The rotors have a diameter of 350mm and they are powered by two electric motors. By spinning the rotors in opposite directions the flow shown in Figure (12) is generated. As indicated by the two laser beams and the coordinate system shown in Figure (12), the radial component of the flow velocity and acceleration were measured in the middle of the tank. In this measurement, data of the order of $6 \cdot 10^5$ burst signals have been obtained. To compare this result to that found by the strip detectors at a Taylor microscale Reynolds- number of approx. 690 the normalized probability density functions (PDF) were calculated. The functions to normalize the velocity and the acceleration are given in equation (9).

$$v_{normalized,i} = \frac{v_i - < v >}{< v^2 >^{\frac{1}{2}}}, \quad a_{normalized,i} = \frac{a_i - < a >}{< a^2 >^{\frac{1}{2}}} \tag{9}$$

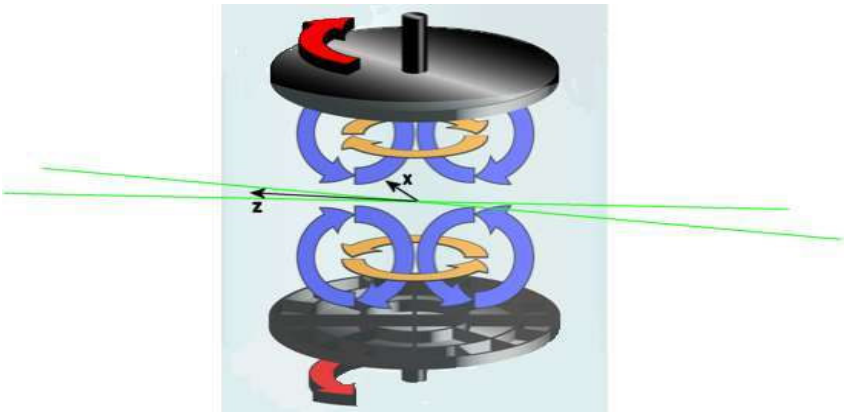

Figure 12: Flow in the turbulence generator

Previous results indicate that the normalized PDF of the velocity and the acceleration are independent of the flows Reynolds number. The normalized PDF of the velocity exhibits a Gaussian shape and the distribution of acceleration follows the function given in equation (10).

$$P(a) = C \cdot \exp\left(\frac{a^2}{\left(1 + \left| a \frac{\beta}{\sigma} \right|^{\gamma} \sigma^2 \right)} \right) \qquad (10)$$

In this equation the parameters are $C = 0{,}733$, $\beta = 0{,}513$, $\gamma = 1{,}6$ and $\sigma = 0{,}563$.

Figure (13) shows the velocity and the acceleration distributions using the laser Doppler technique. For comparison a Gaussian curve is plotted as a dotted line in both diagrams and the solid line in the acceleration PDF corresponds to previous measurements using the silicon strip detectors (La Porta et al. 2001).
The shape of the measured velocity PDF fits the Gaussian curve very well. The measured acceleration PDF resembles previous measurements in the region $-4 < a / < a^2 >^{1/2} < 4$. For larger accelerations the curve exhibits a Gaussian shape. This leads to the conclusion that the acceleration measurement with the laser Doppler system is sensitive to noise. In the inner region there are reliable acceleration values calculated from burst signals with a very good signal-to-noise ratio (SNR) and the outer regions correspond to acceleration estimates made from burst signals with poor SNR.

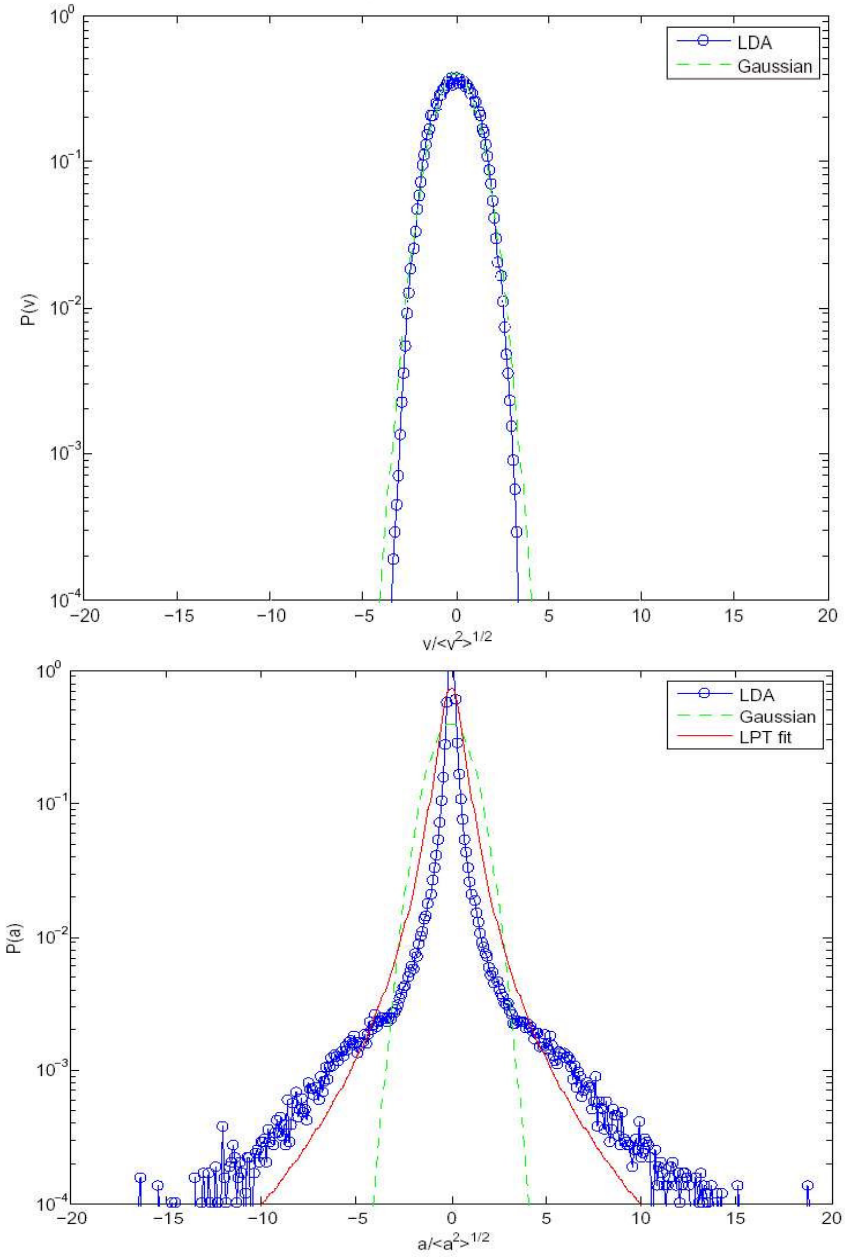

Figure 13: PDFs from turbulence generator measurement

To improve the acceleration measurements the signal processing was extended by an algorithm that removes burst signals with poor SNR from the statistics. Figure (14) shows the same result using this extended program. The acceleration PDF now agrees with previous measurements very well. The velocity PDF shows a bimodal distribution with a sharp dip at low velocities. This corresponds to the well documented velocity bias.
With the extended signal processing an RMS value of about 20m/s² was measured for the acceleration in the turbulent generator measurement. This is the same value that was found previously.

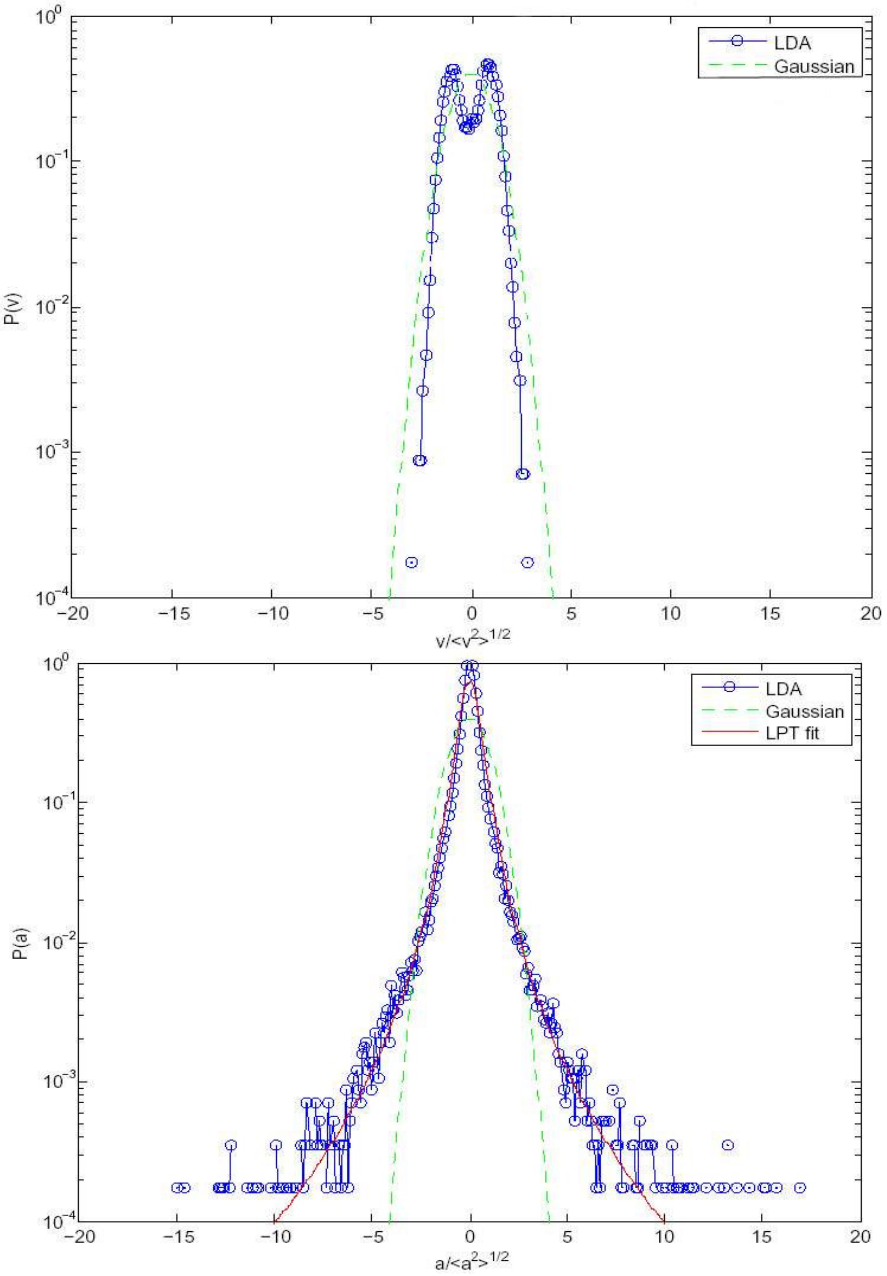

Figure 14: Filtered PDFs from turbulence generator measurement

5 CONCLUSIONS

In this project a laser Doppler system that can measure not only the flow velocity but also its Lagrangian acceleration was successfully built and tested.
To obtain the velocity and the acceleration a model signal is fitted to the measured burst signal. The required values for the velocity and the acceleration result out of a parameter estimation procedure.
With careful alignment and an improved signal processing, an RMS value of less than 50m/s² could be achieved in the turbulent flow studied. This is a very low value considering the corresponding small change of the velocity within the measurement volume and the high accelerations in turbulent flows.
The first validation measurements have shown that it is possible to measure Lagrangian acceleration with the laser Doppler system. The agreement between the laser Doppler measurement results and the results gained using particle tracking with silicon strip detectors is especially convincing.

6 ACKNOWLEDGEMENTS

The financial support by the German Academic Exchange Service (DAAD), the National Science Foundation (NSF) and the German Research Foundation (DFG) are gratefully acknowledged. Furthermore the authors would like to thank H. Xu, Ph. D., N. Ouellette, Ph. D. and K. Chang, M. Sc. for the contribution to our good work.

References

H. E. Albrecht, M. Borys, N. Damaschke, C. Tropea: Laser Doppler and Phase Doppler Measurement Techniques. Springer, 2003

N. T. Ouellette, H. Xu and E. Bodenschatz (2005): A quantitative study of three-dimensional Lagrangian particle tracking algorithms. Exp. in Fluids, DOI: 10.1007/s00348-005-0068-7

G. A. Voth, A. La Porta, A. M. Crawford, E. Bodenschatz, C. Ward, and J. Alexander (2001): A silicon strip detector system for high resolution particle tracking in turbulence. Rev. Sci. Instrum. 72(12), pp. 4348-4353

A. La Porta, G. A. Voth, A. M. Crawford, J. Alexander and E. Bodenschatz (2001): Fluid particle accelerations in fully developed turbulence. Nature vol. 409, pp. 1017-1019

G. A. Voth, A. La Porta, A. M. Crawford, J. Alexander and E. Bodenschatz (2002): Measurement of particle accelerations in fully developed turbulence. JFM vol. 469, pp. 121-160

B. Lehmann, A. Helbig, and C. Hassa (1990): LDA method to measure the acceleration of particles and the curvature radii of particle trajectories. In Proc. 5th Int. Symp. on Appl. of Laser Techn. to Fluid Mechanics, Lisbon, Portugal, paper 22.3.

B. Lehmann and J. Helbig (2000): Local acquisition of mean and turbulent fluid acceleration in highly turbulent flow by the means of laser-Doppler velocimetry. In Proc. 10th Int. Symp. on Appl. of Laser Techn. to Fluid Mechanics, Lisbon, Portugal

B. Lehmann, H. Nobach, and C. Tropea (2002): Measurement of acceleration using the laser Doppler technique. Meas. Sci. Technol. 13(9), pp. 1367-1381